

SATELLITE OBSERVATIONS OF TEMPORAL TERRESTRIAL FEATURES

By George Rabchevsky
Allied Research Associates, Inc.

Abstract

In the 11 years since the launch of the first orbiting meteorological Television and Infrared Observation Satellite (TIROS I) on April 1, 1960, over 1 million pictures of the earth have been recorded by 25 weather satellites. During the 10 manned orbital flights of the Gemini program, the astronauts took over 2400 seventy mm color photographs; coverage obtained from Apollo VI, VII, and IX missions comprises a total of 2100 pictures. This coverage, at various times, scales, and geographic locations, has given us a unique look at the dynamic features of the earth on a daily, weekly, seasonal, and yearly basis. This report will review some of these observations and their utility to the various earth science disciplines.

Acknowledgments

The author gratefully acknowledges the help of Mr. John E. Sissala in the preparation of this paper, which is based largely on his talk entitled, "The Utilization of the Various Time Scales of Meteorological Satellite Observations to Monitor Terrestrial Changes," presented at the First Western Space Congress, sponsored by the Vandenberg Scientific and Technical Societies Council, held on October 27-29, 1970, at Santa Maria, California.

The manuscript was also reviewed and useful comments made by the following individuals, whose cooperation is also gratefully acknowledged: Mr. Don Kulow, U.S. Geological Survey, EROS Program; Mr. Morris Deutsch, U.S. Geological Survey, EROS Program; and Dr. Paul McClain, National Oceanic and Atmospheric Administration (NOAA), National Environmental Satellite Center.

Introduction

The photographic coverage of the earth's surface obtained from the Gemini and Apollo missions ranges in resolution from 30 to 200 ft. Unlike the meteorological satellite coverage, however, the

photography¹ is not repetitive and is confined only to the lower latitudes. On the other hand, the experimental, meteorological, polar-orbiting satellite (Nimbus) and the improved TIROS operational meteorological satellite (ITOS) permit two observations of any point on the earth every 24 hours, once during the daytime and once during the nighttime. An even more frequent daily coverage is provided by the Applications Technology Satellite (ATS) series, placed in geosynchronous² stationary orbit 22 300 miles above the equator. Every 20 min a picture is taken of diurnal conditions over the Atlantic and Pacific Ocean regions. Their application to nonmeteorological studies, however, is not yet fully explored.

Application of satellite data to earth resources and environmental studies depends largely on the resolution³ of the photographs and imagery. Only data from the Nimbus satellite series is adequate for this purpose, besides the Gemini and Apollo photography. Nimbus satellites with ground resolutions from 0.5 to 7.5 n. mi. at the subpoint have given us a new perspective to view our continually changing atmospheric and terrestrial environment.

1. Photography - The production of a permanent or ephemeral image of a subject on a medium which is directly exposed to electromagnetic radiation emitted or reflected from the subject, or transmitted through the subject, and is affected by the radiation in direct proportion to the emission, reflection, or transmission characteristics of the subject.
2. Geosynchronous - Same as earth synchronous.
3. Resolution - The minimum distance between two adjacent features, or the minimum size of a feature, which can be detected by a photographic or an imaging system. For photography, this distance is usually expressed in line pairs per millimeter recorded on a particular film under specified conditions; as displayed by radar, in lines per millimeter. If expressed in size of objects or distances on the ground, the distance is termed "ground resolution."

When two or more satellites are in orbit simultaneously, the capability to view each point on the earth increases. This capability has not been used extensively yet, although it offers attractive advantages for some applications. Many features would not exhibit any change even if viewed from the same angle each day, because the parameters being sensed do not change significantly during short time scales. Movements along geologic faults or polar ice shelf boundary changes are an example of this situation. Thus, while changes of some features may be observed daily or more often, it is at times necessary to make longer temporal comparisons of imagery to determine the significance and amount of change. Table 1 summarizes some of the temporal terrestrial features and the time scales of observations required for their detection.

The Earth Resources Technology Satellite (ERTS) is planned for launch by NASA for March of 1972. The expected 18-day repeat coverage from ERTS will enable us to map dynamic terrestrial features (coastal processes, erosion, floods, vegetation bloom) and classify events and landforms (geologic hazards, drainage networks, lakes) on a regional scale for the first time. The presently available satellite data are meanwhile generating background studies for future more detailed and local applications of the ERTS photographs and imagery.⁴

Oceanography

Sea surface temperature observations are proceeding actively using satellite radiometers.⁵

4. Imagery - The pictorial representation of a subject produced by electromagnetic radiation emitted or reflected from a subject, or transmitted through the subject, and detected by a reversible-state physical or chemical transducer whose output is capable of providing an image.
5. Radiometer - A radiation-measuring instrument having substantially equal response to a relatively wide band of wavelengths in the infrared region. Radiometers measure the difference between the source radiation incident on the radiometer detector and a radiant energy reference level.

Over cloud-free ocean regions, surface temperatures have been measured with an accuracy of $\pm 2^\circ \text{K}$ ⁶ [1,2,3]. The Nimbus and ITOS satellites have the capability to sense the ocean surface temperature every 12 hours.

Current Boundaries. Nimbus radiometers have sensed thermal boundaries of major ocean currents (Fig. 1). Changes in these boundary positions have been observed on a daily and weekly basis. Boundary changes along the north wall of the Gulf Stream have been computed for a 2-month period using those data [4]. Since currents could be utilized or avoided to save shipping time, ship routing will depend on accurate knowledge of the location, extent, and velocity of currents. It has also been suggested that spaceborne oceanographers might be able to see current shears due to modifications of wave characteristics, waves from islands, undersea topography, color due to contaminants, or some other factors [5].

Ocean Upwelling. Some areas of upwelling have been studied in detail. Changes in their thermal patterns have been correlated with concentrations of fishing and phytoplankton activities [6]. A 3-day interval upwelling pattern change of the Somalian coast is illustrated in Figure 2. Yearly views of this area indicate the recurrence of this thermal pattern during the same season, suggesting that the commencement of upwelling can be monitored with satellite data [7].

Analyzed at hourly intervals just west of the Galapagos Islands, ATS III pictures have suggested the presence of upwelling within the sunglint patterns [8,9]. Similar anomalous patterns in areas of sunglint are usually observed daily by the Nimbus and ITOS satellites (Fig. 3).

The deep blue water along the upper west and east coasts of Taiwan (Fig. 4) are areas of upwelling, potential sources of new fishing grounds. Timely observation of such drastic temperature changes is imperative for proper management and conservation of ocean resources.

Sea State. Unusual dark patches observed within the sunglint patterns on Nimbus and other satellite photographs seem to be also due to areas

6. K - identifies Kelvin thermometric scale; 0°K is absolute zero, -273.13°C or -459.4°F .

of calm water in the midst of rougher sea surfaces (Fig. 3). Hourly reflectance changes of these dark spots have also been observed on the ATS imagery. It has been suggested that these dark spots may be correlated with areas of calm water and upwelling [8,9].

The complex nature of the ocean surface is revealed in Figure 5, as seen by the crew of Apollo 7 on October 15, 1968, from 100 miles in space. The water around the islands of Socotra and the Brothers are caught in the sun's reflection, revealing a complex surface phenomenon impossible to view by ordinary means. Situated just off the east African coast and north of one of the strongest upwelling areas in the world, the islands form a deflective barrier to the northeastward movement of the cold, upwelled water. The vortices, slicks, swells, and other lines which are visible reveal current direction, internal waves, and regions of convergence and divergence. Repetitive observations of such features are invaluable in oceanographic research.

Polar Pack Ice Boundaries. Pack ice boundaries have been established for both polar seas using satellite imagery [10,11,12]. Month-to-month and year-to-year changes in the Antarctic pack ice boundaries north of the Weddell Sea have been determined from Nimbus II and III pictorial imagery (Fig. 6) [13,14].

Arctic ice and water temperature boundaries have been determined using satellite data [15]. Discrimination of older ice from newer ice near the ice and water boundary is also possible, as is detection of weekly and monthly thermal changes in these boundary positions. Current technology cannot provide a continuous or integrated measure of ice cover. Present estimates are based almost entirely on point samples, often obtained with considerable difficulty under adverse conditions. Better information is needed on the total quantity of water stored as snow and ice in a given area, and repetitive sampling from satellites may provide such information.

Ice Concentrations. Polar (and temperate climate) ice concentrations can be extracted from satellite data [11,15,16,17]. Daily and weekly changes at specific locations have been observed and corroborated with conventionally gathered visible and infrared⁷ data.

7. Infrared - Pertaining to or designating the portion of the electromagnetic spectrum with wavelengths just beyond the red end of the visible spectrum, such as radiation emitted by a hot body. Invisible to the eye, infrared rays are

In general, new, thin ice cannot be detected unless covered by snow. Ice concentrations from 1 to 0.3 are often evaluated as ice free because of limitations of satellite system resolutions. There is usually good agreement with ice charts of ice amount between 4 and 0.7 and excellent agreement of ice amounts greater than 0.7. Changes of concentration from one of these classes to another have been reliably determined.

The British Arctic Survey (BAS) has been receiving regular ESSA satellite photo coverage of the Antarctic Peninsula area since 1967. These pictures have proven to be of real benefit to observe the distribution of pack ice to facilitate the passage of the Survey's ships to Antarctic stations. The ships' ice reports are continually used with the satellite pictures to develop confidence in the ice amounts derived from satellite data.

Off-Shore Leads. The formation of polar off-shore leads has also been observed on satellite photographs (Fig. 7). An interesting phenomenon is the annual development of leads at specific locations at approximately the same time of year. Nimbus I, II, and III in late August 1964, 1966, and 1969 observed a lead development off the east coast of the Antarctic Peninsula in the Weddell Sea [18]. Similar observations have been made in the Arctic.

These features can be used as corridors by ship traffic to reach remote scientific stations. The seasonal behavior of such leads could be easily monitored through repetitive satellite observations. The frequency of such observations would increase during the spring and fall seasons (daily observation) and decrease during the rest of the year (monthly observations).

Iceberg and Ice Floe Tracking. Large tabular icebergs have been observed and their movement followed in Antarctica (Figs. 8 and 9), while large ice floes have been tracked off the east coast of Greenland [19]. The first tabular iceberg to ever be viewed from space was seen by Nimbus I in 1964 at the junction of the Filchner Ice Shelf and the Antarctic Peninsula [20]. Nimbus III views of this area in 1969 revealed that this 70-n.-mi.-long iceberg had moved into the ice pack, leaving an indentation in the coast-

detected by their thermal and photographic effects. Their wavelengths are longer than those of visible light and shorter than those of radio waves, light rays whose wavelength is greater than 700 nm milli-microns.

line identical to the iceberg's shape. The Environmental Science Services Administration (ESSA) satellite observations of this area during the intervening years would probably establish the time of separation and possibly the rate of movement of this feature through the Weddell Sea.

Two giant icebergs were observed by the ESSA-III satellite during the 1967-68 Antarctic summer. They were moving westward along the coast in the Weddell Sea. Movement and size of these icebergs were compared with reports from Antarctic stations. It is suggested that one or both of these icebergs may be derived from that which calved from the Amery Ice Shelf in late 1963 [21].

Hydrologic Applications

Snow Boundaries. Useful snow information has been extracted from satellite data. Daily and weekly changes of the snowline in the upper Missouri-Mississippi River Valley were mapped from satellite data with very good agreement with the ground derived snowline [22]. Figure 10 is an example of a snowfall boundary change along the eastern part of the U.S.

Weekly changes in the U.S. snow boundaries have been automatically determined from ESSA and the Advanced Vidicon (television) Camera System (AVCS) imagery through the use of a computer which stores all reflectance values, for each data point, in digital form. Upon command, an array of the lowest reflectance for each data point is displayed as a Composite Minimum Brightness (CMB) chart [10]. Snow and ice boundaries are readily apparent, as the transient cloud patterns are eliminated by this procedure.

Weekly snow-coverage changes monitored by meteorological satellites in river basins in the southern Sierras of California have correlated within ± 5 percent of aerial snow survey measurements [23]. Figure 11 is an Apollo IX view of the southern Sierras. Similar photographs from the forthcoming ERTS system will greatly enhance the mapping of biweekly and monthly scales.

Monthly and annual changes of snow coverage in the Himalaya and Hindu Kush Mountains have been observed but, as yet, no quantitative evaluation of these changes has been made (Figure 12) [24]. Similarly, the three Nimbus IV Image Dissector Camera (TV) System (IDCS) pictures, taken over a period of 1 month (Fig. 13), show a rapid decrease in snow cover on the peninsula of Kamchatka.

Inland Lake Temperatures. The seasonal progression of the average surface temperature of Lake Michigan has been obtained using the Nimbus High Resolution Infrared Radiometer (HRIR) data [25]. Figure 14 shows Lake Michigan temperature patterns during 1966 from Nimbus II HRIR. Although Nimbus surveyed the Lake Michigan area nightly, observation of the entire lake was limited on many occasions by cloud cover and by sunlight interference [26]. Such observational constraints will be present also in the anticipated ERTS data.

Reservoir Accumulation. Water accumulation behind major dams has been repeatedly observed by meteorological satellites. Change in tone and pattern related to water accumulation behind the Aswan Dam has been observed by Nimbus I, II, and III satellites between 1964 and 1969.

When the Gemini IV photograph was taken in June 1965 (Fig. 15), the Aswan High Dam was beginning to fill, as is evident in the tributary canyons with water in them. In Figure 16, Lake Nasser, the name for the immense body of water backed up by the Aswan Dam, dominates the foreground of this view of Egypt photographed by Apollo IX astronauts in March of 1969. Nimbus satellite systems have recorded images of the Lake Nasser area since September 1964. The increase in lake size can be seen between the 1964 conditions (Fig. 17A) and 1969 (Fig. 17D) [27].

Repetitive observations of similar reservoir fill-ups would be more frequent during the initial phases and would decline to monthly and yearly monitoring after their completion.

Flooding and Drought. The Nimbus and ITOS television and infrared imaging sensors have the capacity to monitor surface moisture and extent of water bodies. The effects of a spring flood of the Ouachita River on ground water migrations and vegetation blooms have been detected by Nimbus 3 HRIR sensors (Fig. 18). The Apollo IX near-infrared image of the area (Fig. 19), taken March 9, 1969, shows this area at the height of the flood when about 165 mi² were inundated. From the analysis of the digitized Nimbus III HRIR grid-print reflectance maps⁸ [14, 18], it was concluded that this flood had more effect on the intensively cultivated area along the Mississippi River, with a lesser effect on the more forested highlands in the western half of the map. Weekly and monthly observations revealed the lingering effects of this flood on the

8. Grid-print maps — Computer-produced maps of temperature or reflectance values.

ground water migrations, water table oscillations, and vegetation responses to the above-mentioned conditions, several months after the flood.

Drought conditions have also been observed by the Nimbus III HRIR daytime satellite sensors in the lower Mississippi Valley. Where severe drought conditions affected this area during the summer of 1969, a general increase in terrain reflectance is observed (Fig. 20). The moisture decrease, from May 22 to August 9, resulting from a decrease in rainfall, affected the vegetal cover (wilted vegetation, poor crop yield) and soil texture; the radiometer, in turn, integrated those changes as higher reflectances. Similarly, a reversal to a lower relative reflectance by September 12 was a response to moisture added to the ground from increased rainfall [13, 14, 18].

Vegetation Boundaries. In Figure 21 the reflectance changes observed in the three Nimbus III HRIR daytime images of Western Africa correlate roughly with the broad vegetation zones of the tropical forest, Savanna-Forest, and Savanna Grasslands that belt the West African Continent south of the Sahara Desert. These regional vegetation boundaries correspond to changes in soil moisture, as a response to seasonal meteorological conditions [13, 14]. Mapping of such dynamic features will be greatly enhanced by the availability of repeat satellite coverage, since the vegetation boundaries fluctuate latitudinally from season to season. This figure illustrates once more that conventional vegetation boundary maps are inadequate for the depiction of similar temporal events.

Geographic and Geologic Applications

Map Revisions. Geographic maps of polar areas have been updated using the Nimbus satellite imagery [28]. Ice front locations in Antarctica have been revised [29]. Mount Siple was repositioned 2 deg west, and a mountain group in the Kohler Range was eliminated as it had been positioned differently by two different expeditions (Fig. 22). Nimbus I and II imagery has supplemented conventional data in the preparation of maps of portions of Tibet and China [30].

Differential reflectance effects of snow occasionally highlight previously nondiscernible ground features. Repetitive satellite observations are able to take advantage of this fact. A new vegetation boundary was suggested in Canada because the seasonal effects of snow highlighted the boundary between areas of less than 30 percent and more than 30 percent woodland cover [31]. Midwinter observations, with too much

snow, obscured the boundary; whereas late spring observations had too little snow. The optimum observation period existed for only 2 months.

The aid of repetitive observations of snow cover in geologic mapping is illustrated in Figure 23. Through the analysis of a fresh snow pattern, photographed by the Nimbus I TV camera, a fault in the East Sayan Mountains of the U.S.S.R. was detected. The fact that a few weeks earlier or later this pattern would have been obscured by a lack of snow or too much of it reveals how unusual and unexpected the benefits may be from the analysis of satellite repetitive observation photographs.

Volcanic Activity. Cases of effusive volcanic activity have been recorded by orbital infrared systems, Kilauea and Etna by the Nimbus I satellite and Surtsey by the Nimbus 2 satellite. Surtsey is the best documented and appeared as a minute spot on more than eight separate orbits of the Nimbus HRIR between August 20 and October 30, 1966 (Fig. 24). Calculations indicate that only about 3 percent of Surtsey's total thermal energy left the earth's atmosphere as radiant energy [32]. Nevertheless, the repeated detection of Surtsey demonstrates that radiation from effusive volcanic events of similar magnitude can be detected and monitored from earth orbit with appropriate systems and repetitive looks over an area.

In another instance, a plume resulting from the eruption of the Beerenberg Volcano on Jan Mayen Island was observed by the Nimbus IV IDCS camera and daytime HRIR system, beginning on September 21, 1970 (Fig. 25). This observation demonstrates once more the significance of frequent repetitive satellite observations in improving our understanding of natural processes of the earth and atmosphere [33].

The Nimbus IV satellite relayed the temperature of steam emitted from the snowcapped Mount Rainier volcano in Washington [34]. This is the first time that volcanic activity information had been transmitted on a daily basis by a satellite. In the future, pictorial information may accompany data from similar Interrogation, Recording and Location Systems (IRLS).

Playa Changes. Western U.S. playas have been examined from space and evaluated as potential aircraft landing sites. Changes in surface moisture conditions would affect their availability as landing sites. Repetitive observations correlated with ground measurements could establish a basis for satellite determination of the daily activity of these

playas as landing sites. Research along these lines has shown the value of satellite pictures although improved resolutions are required for more detailed information.

Figure 26 is a Nimbus I AVCS photograph taken over northwestern Nevada. It shows a variety of playa surface conditions, ranging from hard, dry crusts (locations 2, 3, 6, 7, 16 and 19) to soft, dry, friable surfaces (locations 5, 8, 10, 14 and 15). Neal [35] concludes that the utility of Nimbus images in playa studies is limited, but they nevertheless contain usable information when used in conjunction with higher resolution photography, such as that from the Gemini mission (Fig. 27). Consequently, repetitive high-resolution imagery from the ERTS will allow continuous monitoring of playa surfaces on an 18-day basis, at least when the cloud cover is absent.

Delta Sedimentation. Delta sedimentation plumes have been observed on Nimbus I imagery at the mouth of the Colorado River in the Gulf of California and at the mouth of the Tigris-Euphrates Rivers in the Persian Gulf (Fig. 28). ATS III has observed this feature off the mouth of the Amazon River (Fig. 29). Numerous examples of coastal and inland lake deltaic sedimentation have also been photographed by the Gemini and Apollo (Fig. 30) astronauts. Sedimentation is an extremely dynamic process and, in order to be monitored effectively, should be observed on a weekly and, at times, even on a daily basis. Presently available daily coverage from meteorological satellites is too poor for such purposes. The ERTS program will improve the situation somewhat; however, more than biweekly coverage is necessary for the monitoring of such temporal terrestrial events, as sedimentation, crop maturation, or volcanic eruptions.

Miscellaneous Observations

Duststorms. Sahara Desert duststorms have been observed daily on Nimbus satellite imagery (Fig. 31). No intensive investigation has yet been performed to determine the frequency at which these phenomena should be observed, or the quantitative information that could be obtained from the Nimbus imagery. The ATS III photographed a similar dust-storm a year earlier (1969) over the same region, monitored on an hourly basis. To date, however, eolian processes of erosion, deposition, and associated landforms have not been studied with the aid of Nimbus or ATS data.

Ship Plumes. Ship condensation trails have been observed on satellite imagery and documented with ground observations [36]. These features, where and when they exist, can be charted. The present civilian utility of this information is not very great, although this does have implications for monitoring of contrail persistence from the future supersonic air transports in relation to atmospheric pollution.

The long, thin, anomalous cloud bands in the Nimbus III IDCS pictures, in Figure 32, are most probably ship plumes or "trails." Daily and weekly observations of these features from space would greatly enhance the inventorying of oceanic transport activities and ship-traffic routing. Ship plumes have also been photographed by Gemini and Apollo astronauts, and recorded by ITOS and ATS systems.

Forest and Brush Fires. Smoke from large fires in Alaska has been observed on ESSA satellite imagery [37]. Figure 33, from the Nimbus IV IDCS, shows smoke plumes from major brush fires in southern California. Figure 34 shows similar fires over the mouth of the Zambezi River at Mozambique, East Africa, photographed by Apollo VII astronauts.

Even though forest fires have been photographed from space, present poor resolution of the meteorological satellite sensors and nonrepetitive observations by the Gemini and Apollo astronauts preclude operational monitoring of the effects of such fires on resources economics and atmospheric pollution.

Conclusion

The list of temporal terrestrial features presented in this paper and summarized in Table 1, as observed from space, is not exhaustive. The need for repetitive observations of dynamic features is, however, self-evident if we ever hope to fully understand the changes affecting our broad-scale, repetitive views of the earth from future space missions, such as ERTS, for example, will be especially useful for a wide variety of regional inventory and planning programs. Such inventories may then be used to identify areas of change so that acquisition of more precise information by aircraft or ground methods could be planned.

References

1. Warnecke, G., McMillin, M., and Allison, L. J.: Ocean Current and Sea Surface Temper-

- ature Observations from Meteorological Satellites. Goddard Space Flight Center, Greenbelt, Md., NASA TN-D-5142, 1969.
2. Smith, W. L., Rao, P. K., Koffler, R., and Curtis, N. R.: The Determination of Sea-Surface Temperature from Satellite High Resolution Infrared Window Radiation Measurements. *Monthly Weather Review*, vol. 98, no. 8, 1970, pp. 604-611.
 3. Warnecke, G., Allison, L. J., McMillin, L. M., and Szekelda, C.: Remote Sensing of Ocean Currents and Sea Surface Temperature Changes Derived From the Nimbus 2 Satellite. *Your Physical Oceanography*, vol. 1, no. 1, 1971, pp. 45-60.
 4. Greaves, J. R., Willand, J. H., and Chang, D. T.: Observations of Sea Surface Temperature Patterns and Their Synoptic Changes through Optimal Processing of Nimbus II Data. NASA Final Report, Allied Research Associates, Inc., Contract No. NASW-1651, 1968.
 5. Woods Hole Oceanographic Institute: Oceanography From Space. WHOI, Ref. no. 65-10, 1965.
 6. Szekielda, K. H.: The Effect of Cyclonic and Anticyclonic Water Movements on the Distribution of Organic Matter. Goddard Space Flight Center, Greenbelt, Md., NASA X-622-70-40, 1970.
 7. LaViolette, P. E., and Seim, S. E.: Satellites Capable of Oceanographic Data Acquisition - A Review. U.S. Naval Oceanographic Office Technical Report 215, Washington, D. C., 1969.
 8. Bowley, C. J., Greaves, J. R., and Spiegel, S. L.: Sunlint Patterns: Unusual Dark Patches. *Science*, vol. 165, 1969, pp. 1360-1362.
 9. McClain, E. P., and Strong, A. E.: On Anomalous Dark Patches in Satellite-Viewed Sunlint Areas. *Monthly Weather Review*, vol. 97, no. 12, 1969, pp. 875-884.
 10. McClain, E. P., and Baker, D. R.: Experimental Large-Scale Snow and Ice Mapping with Composite Minimum Brightness Charts. Technical Memorandum NESCTM-12, National Environmental Satellite Center, Washington, D. C., 1969.
 11. Nelson, H. P., Roberts, S. N., and Roberts, T. D.: Sea Ice Reconnaissance by Satellite Imagery. Final Report, NASA Contract No. N-62306-68-C-0261, Institute of Arctic Environmental Engineering, University of Alaska, College, Alaska, NASA Contract No. N-62306-68-C-0261, 1970.
 12. Swithinbank, C.: Satellite Photographs of the Antarctic Peninsula Area. *The Polar Record*, vol. 5, no. 94, 1970, pp. 19-24.
 13. Rabchevsky, G. A.: Nimbus Satellite Views Hydrologic Conditions. Proceedings of the First Western Space Congress, Part 2, Vandenberg Scientific and Technical Societies Council, Santa Maria, Calif., 1970.
 14. Rabchevsky, G.: Hydrologic Conditions Viewed by the Nimbus Meteorological Satellites. International Remote Sensing Workshop (IRSW), Proceedings, University of Michigan, Ann Arbor, Mich., vol. 2, 1971.
 15. Gibbs, M. E.: The Utilization of Meteorological Satellite Data in Antarctica. U.S. Naval Support Force-Antarctica, Washington, D. C., 1968.
 16. Barnes, J. S., Chang, D. T., and Willand, J. H.: Use of Satellite High Resolution Infrared Imagery to Map Arctic Sea Ice. NASA Contract No. N-62306-68-C-0276, Allied Research Associates, Inc., 1969.
 17. Barnes, J. S., Chang, D. T., and Willand, J. N.: Improved Techniques for Mapping Sea Ice from Satellite Infrared Data. NOAA Contract No. E-67-70(N), Allied Research Associates, Inc., 1970.
 18. Sissala, J. E., and Rabchevsky, G. A.: Terrestrial Changes Monitored by the Nimbus Meteorological Satellites presented at the First Western Space Congress, Vandenberg Scientific and Technical Societies Council, Santa Maria, Calif., 1970.
 19. Sissala, J. E.: Observations of an Antarctic Ocean Tabular Iceberg from the Nimbus II Satellite. *Nature*, vol. 224, no. 5226, 1969, pp. 1285-1287.

20. Popham, R., and Samuelson, R. E.: Polar Exploration with Nimbus. Observations from the Nimbus I Meteorological Satellite, NASA SP-89, 1965.
21. Swithinbank, C.: Giant Iceberg in the Weddell Sea, 1967-68. The Polar Record, vol. 14, no. 91, 1969, pp. 477-478.
22. Barnes, J. C., and Bowley, J.: Snow Cover Distribution as Mapped from Satellite Photography, Final Report. Allied Research Associates, Inc., Contract No. Cnb-11269, 1966.
23. Barnes, J. C., and Bowley, J.: The Use of Environmental Satellite Data for Mapping Annual Snow-Extent Decrease in the Western United States, Final Report. Allied Research Associates, Inc., NASA Contract No. E-252-69(N), 1970.
24. Salomonson, V.V.: Nimbus 3 and 4 Observations of Snow Cover and Other Hydrological Features in the Western Himalayas. Proceedings, International Remote Sensing Workshop (IRSW), University of Michigan, Ann Arbor, Mich., vol. 2, 1971.
25. Sabatini, R. R., and Sissala, J. E.: Project NERO Nimbus Earth Resources Observations, Allied Research Associates, Inc., NASA Technical Report No. 7, Contract No. NAS5-10343, 1968.
26. Sabatini, R. R.: The Feasibility of Using Nimbus HRIR and THIR Measurements for Obtaining Surface Temperature of Lake Michigan. Paper presented at the Great Lakes Conf. Meeting, Toronto, Canada, April 1971.
27. Ackerman, H. J., and Rabchevsky, G. A.: Applications of Nimbus Satellite Imagery to the Monitoring of Man-Made Lakes. Paper presented at the Symposium on Man-Made Lakes, Knoxville, Tenn., May 3-7, 1971.
28. Chief Topographic Engineer: Cartographic and Geologic Uses of Nimbus I AVCS Data. Space Applications, Goddard Space Flight Center, Greenbelt, Md., NASA SP-137, 1965.
29. Waugh, D. V.: Nimbus Satellite Photography Used in Revising 1:5 000 000 Map of Antarctica. American Geographical Society, New York, N. Y., Letter of August 6, 1970.
30. Norin, E.: Nimbus I and II AVCS Used to Identify Points Between Latitude 32 deg and 36 deg N and 72 deg and 90 deg E. Institute of Mineralogy and Geology, University of Uppsala, Uppsala, Sweden, Letter of August 24, 1970.
31. Aldrich, S. A., Aldrich, F. T., and Rudd, R. D.: The Employment of Weather Satellite Imagery in an Effort to Identify and Locate the Forest-Tundra Ecotone in Canada. U.S. Department of the Interior, Geological Survey, Interagency Report NASA-169, Contract W-12589, 1969.
32. Williams, R. S., and Friedman, J.: Satellite Observations of Effusive Volcanism. Journal of the British Interplanetary Society, vol. 23, 1970, pp. 441-450.
33. Merritt, E. S.: Comments on Nimbus 4 Observations of Mt. Beerenberg Volcanic Eruption. Jan Mayen Island, J. of Remote Sensing, vol. 2, no. 2, Sept. 20, 1970.
34. Forrester, F.: Satellite Relays Temperature of Mt. Rainier. U.S. Geological Survey News Release, Oct. 20, 1970.
35. Neal, J. T.: Satellite Monitoring of Lakebed Surfaces in Playa Surface Morphology: Miscellaneous Investigations. Air Force Cambridge Research Laboratories, USAF, AFCRL-68-0133, 1968.
36. Bowley, C. J.: Comments on Atmospheric Requirements for the Genesis of Anomalous Cloud Lines. Journal of the Atmospheric Sciences, vol. 24, pp. 596-597.
37. Parameter, F. C.: Picture of the Month — Alaskan Forest Fires. ESSA, Department of Commerce, Wash., Monthly Weather Review, vol. 97, no. 9, 1969.

TABLE 1. FREQUENCY OF OBSERVATIONS PRESENTLY POSSIBLE AND NECESSARY FOR THE DETECTION OF TEMPORAL TERRESTRIAL FEATURES. ALL THESE CHANGES HAVE BEEN OBSERVED ON ORBITING SPACE IMAGERY, AND MANY HAVE BEEN REPEATEDLY MONITORED BY THE METEOROLOGICAL SATELLITES.

Table 1. Frequency of observations presently possible and necessary for the detection of temporal terrestrial features. All these changes have been observed on orbiting space imagery, and many have been repeatedly monitored by the meteorological satellites.

TEMPORAL TERRESTRIAL FEATURES	OBSERVATION TIME SCALES and REQUIREMENTS						
	Type*	<12hr	12hr	Daily	Weekly	Monthly	Yearly
<u>Oceanography</u>							
Sea Surface Temperatures	P,CS		X	X	X	X	
Current Thermal Boundaries	P,CS		X	X	X	X	
Unwelling	P,CS	X	X	X	X		
Sea State	P,CS	X	X	X	X		
Sedimentation	P,CS			X	X	X	
Water Depth	P				X	X	
Pack Ice Boundaries	P,CS			X	X	X	X
Pack Ice Concentrations	P,CS			X	X		
Formation of Leads	P,CS			X			
Iceberg and Floe Migration	P,CS			X			
<u>Hydrology and Agriculture</u>							
Snowfall Boundaries	CS			X	X	X	X
New Snow Areas	CS		X	X	X		
Snow Depth	PS			X	X		
Inland Lake Temperatures	P,CS		X	X	X	X	
Reservoir Development	PS			X	X	X	X
Flooding	CS			X	X		
Drought	CS				X	X	
Lake Freeze and Melt	CS			X			
Ground Water Migration	C				X	X	
Vegetation Bloom	C				X	X	
Crop Inventories	CS				X	X	
<u>Geology and Geography</u>							
Regional Geologic Mapping	P						X
Volcanic Activity	P,CS	X	X	X	X	X	
Erosion and Deposition	P,CS			X	X	X	
Playa Changes	P,CS			X	X		
Delta Sedimentation	P,CS				X	X	
Urban Growth	P						X
Updating Thematic Maps	P						X
<u>Miscellaneous</u>							
Fire and Smoke Detection	P,CS			X	X		
Dust Storms	CS			X			
Ship Smoke Trails	C			X			
Water and Air Pollution	P,CS			X	X		
Meteorological Conditions	C	X	X	X			

* C = Continuous
P = Periodic
CS = Continuous for seasonal or special events
PS = Periodic for seasonal or special events



NIMBUS III
4 FEBRUARY 1970



NIMBUS III
22 FEBRUARY 1970



ITOS I
22 FEBRUARY 1970



NIMBUS III
26 FEBRUARY 1970

Figure 1. Gulf Stream thermal boundary. These HRIR pictures show the sharp thermal boundary along the north wall of the Gulf Stream. Changes in boundary shape and position are evident. Black picture tones identify the warmest areas. White tones identify the coldest. These pictures were recorded at Goddard Space Flight Center, Greenbelt, Maryland, on an inexpensive ground station (commercially available for about \$5000) especially designed for the direct reception weather satellite pictures.

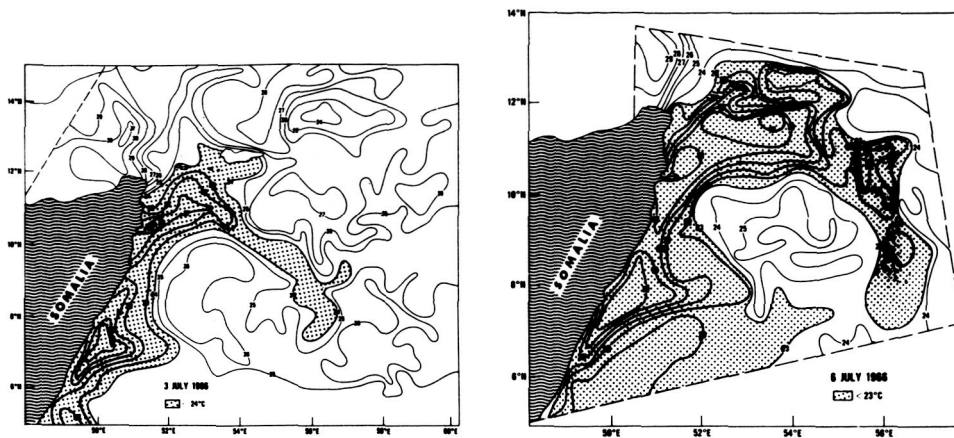


Figure 2. Upwelling changes near the Somalia coast between July 3 and 6, 1966. These two maps show the changing thermal pattern as recorded by the Nimbus II HRIR at the beginning of upwelling near the Somalia coast. The development of the clockwise circulation pattern was correlated with the bloom of phytoplankton.



Figure 3. Sunlight pattern with adjacent anomalous dark spots. This is the central portion of a Nimbus IV IDCS picture taken off the southeast coast of Saudi Arabia on April 15, 1970. The two white x's mark the dark spots which are believed to be areas of calm water and possible upwelling. Southeast Iran is in the upper right corner. (All Nimbus pictures in this report were furnished by the NASA Nimbus Project, Goddard Space Flight Center, Greenbelt, Maryland.)

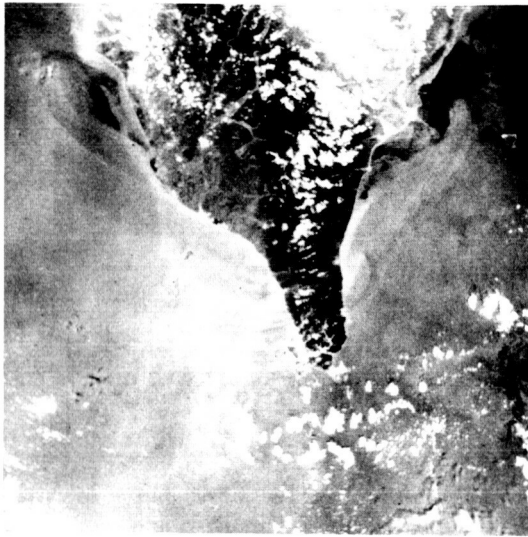


Figure 4. A Gemini X view of ocean surface conditions south of Taiwan (NASA photo).

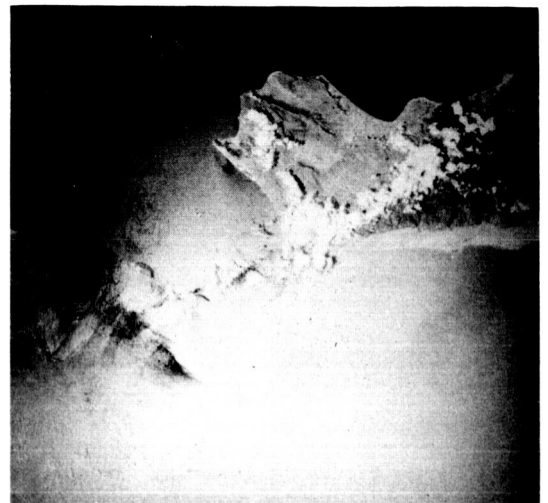


Figure 5. The sun blazed on Socotra Island and the Indian Ocean for this photo. Left of the sunglint, between the big island and smaller ones called the Brothers, a slicklike eddy is darkly outlined. Note the fine, white horizontal line below Socotra. Waves rolling over an undersea shelf 10 miles offshore may have produced it [8] (NASA photo).

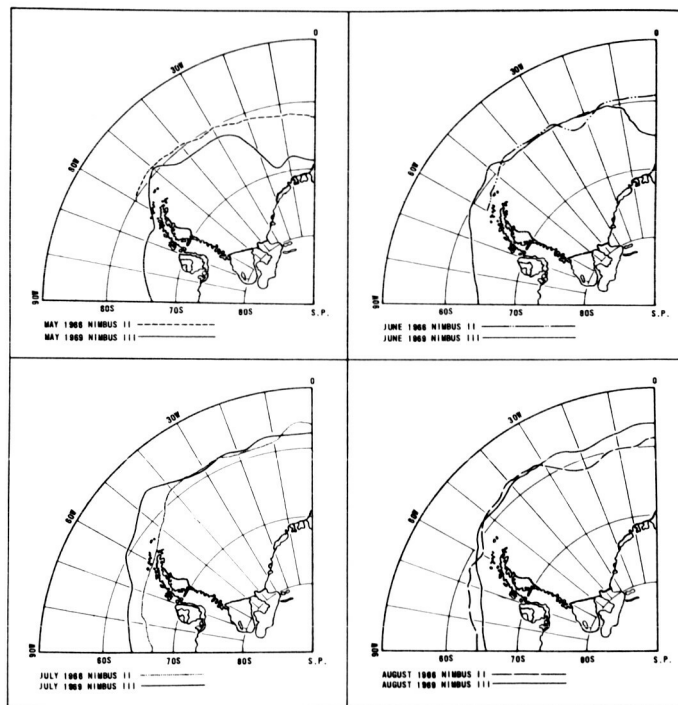


Figure 6. Monthly and yearly fluctuations in Antarctic pack ice boundaries derived from Nimbus satellite data.

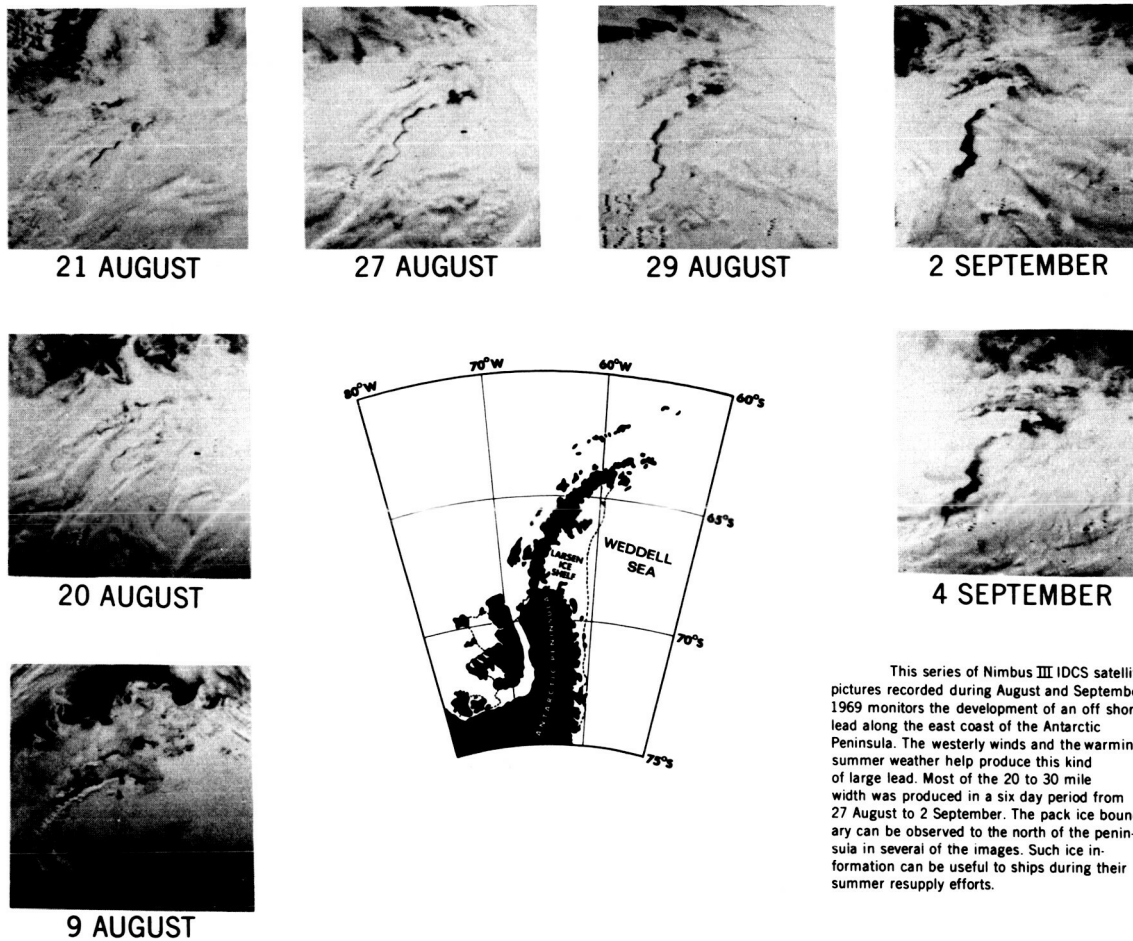


Figure 7. Development of an offshore lead in Antarctica.

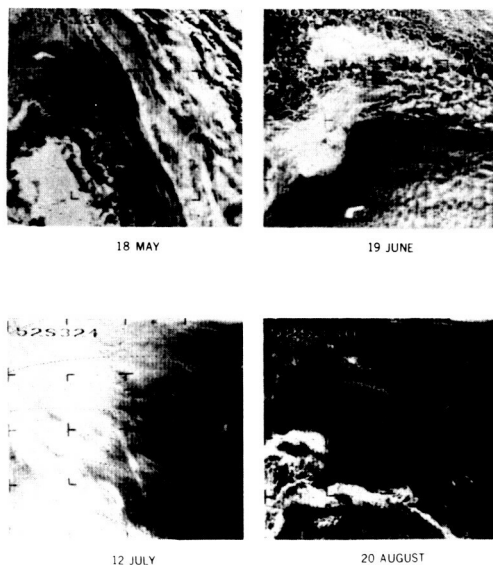


Figure 8. Repetitive observations of a tabular iceberg in the Antarctic Ocean. Nimbus II pictures.

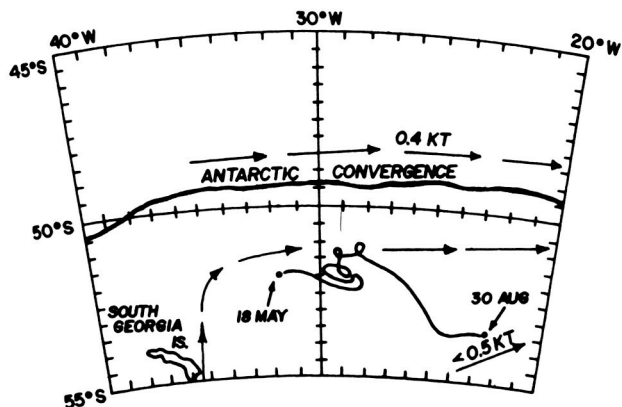
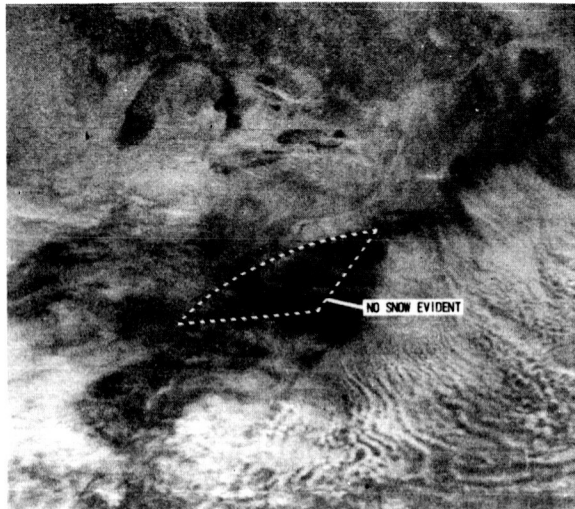
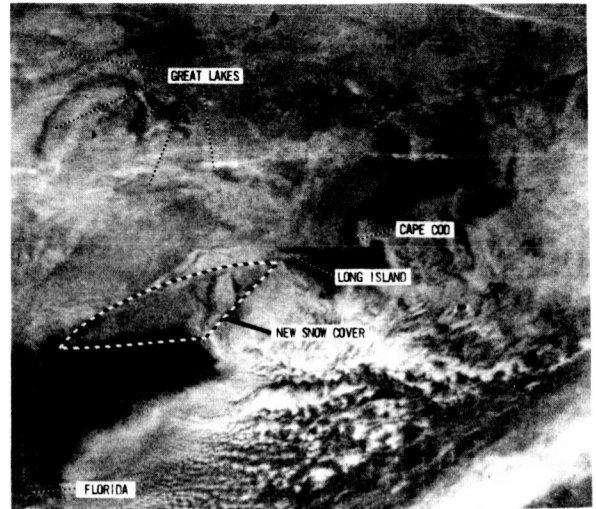


Figure 9. Observed track, from May 18 to August 30, 1966, of the tabular iceberg viewed in Figure 8.



NIMBUS III DIRECT READOUT IDCS ORBIT 3571 5 JANUARY 1970
EASTERN UNITED STATES WITH SNOW COVER



NIMBUS III DIRECT READOUT IDCS ORBIT 3611 8 JANUARY 1970
EASTERN UNITED STATES WITH SNOW COVER

Figure 10. Three-day change in snow pattern. A January 7, 1970, snowstorm dumped new snow in Delaware, Maryland, Virginia, and other eastern areas which had previous snow on the ground.



Figure 11. Apollo IX photograph (March 1969) showing mountain snow cover in southern Sierras region, U.S. The ground resolution in this photograph is of the order of that proposed for future Earth Resources Satellites Systems (NASA photo).

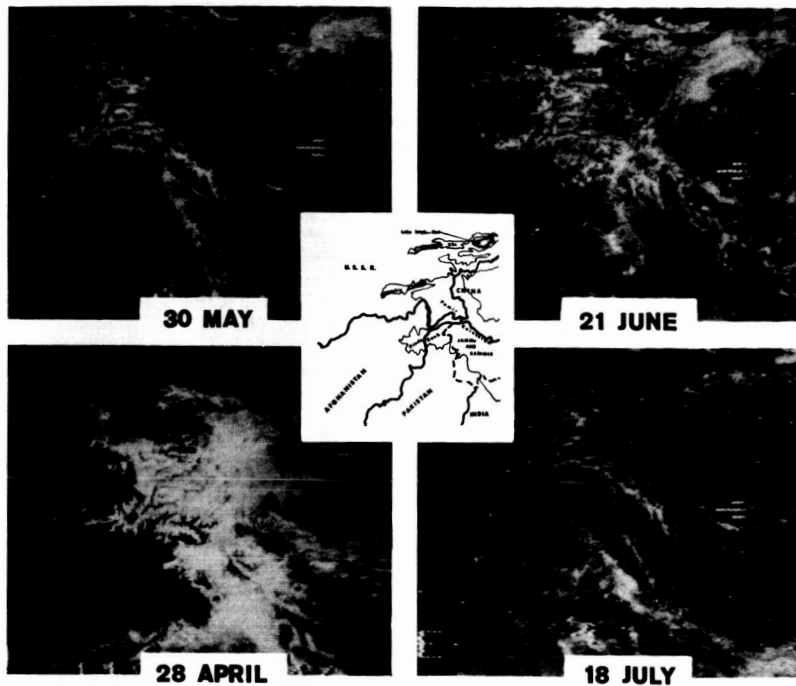


Figure 12. Monthly changes in snow cover in the Hindu Kush and Himalaya Mountains. This temporal sequence of Nimbus III IDCS pictures suggests the utility of a satellite platform to monitor seasonal changes in snow cover. The time and amount of snowmelt is an important input for flood and irrigation planning.

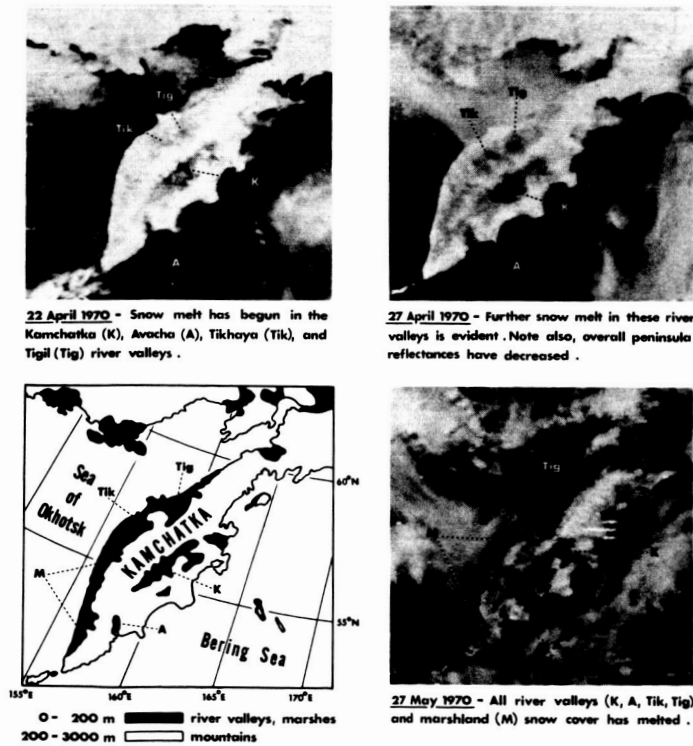


Figure 13. Snowmelt surveillance, Kamchatka, U.S.S.R., Nimbus IV IDCS.

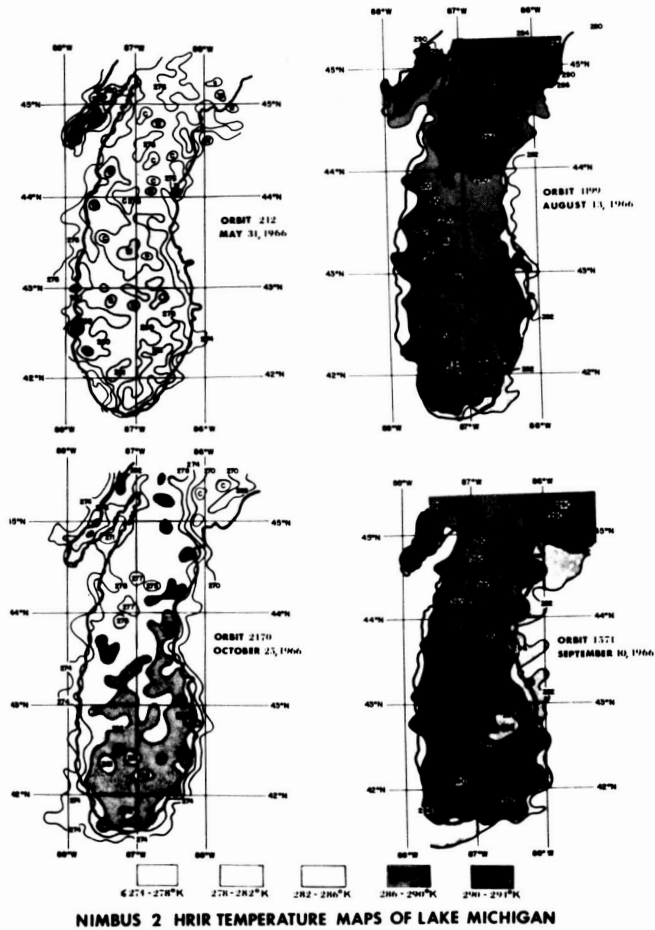


Figure 14. Nimbus II HRIR temperature maps of Lake Michigan derived from digitized data.



Figure 15. Gemini IV photograph of the Aswan High Dam during the initial stages of its filling. The dam is at the top. Part of the area in the center is now flooded by the reservoir (NASA photo).

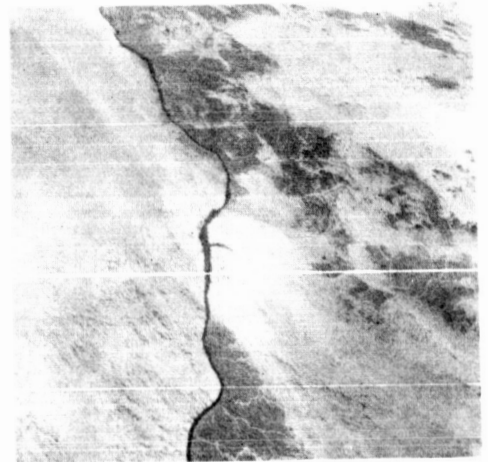


Figure 16. Lake Nasser, a long, immense body of water backed up by the Aswan Dam, dominates the foreground of this view of Egypt. The Red Sea is on the horizon (NASA photo).

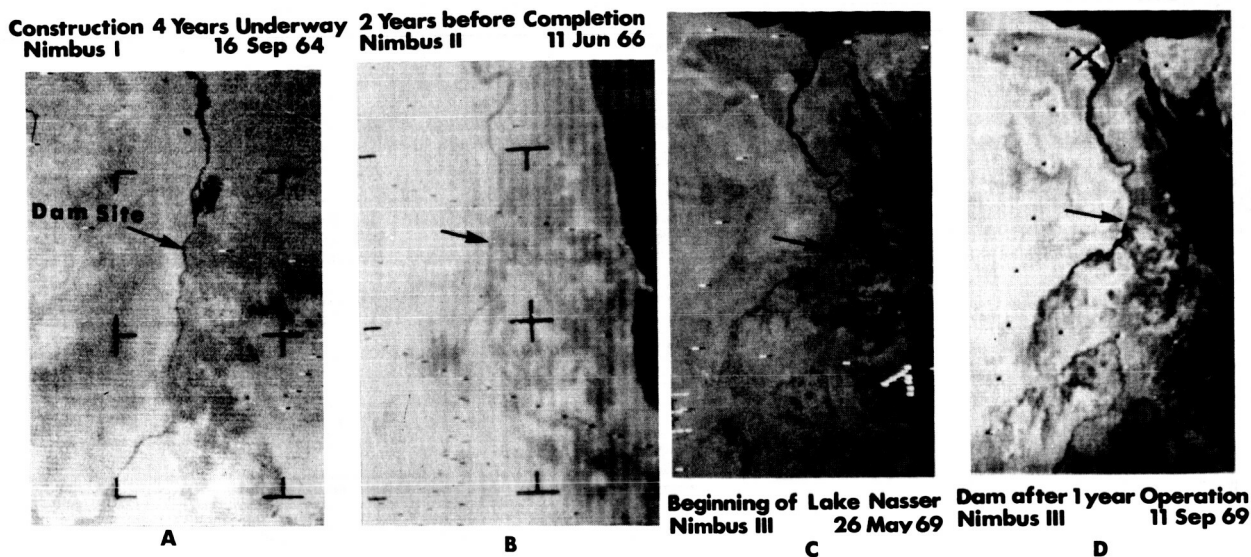


Figure 17. Growth of the Aswan High Dam monitored by Nimbus satellite cameras.

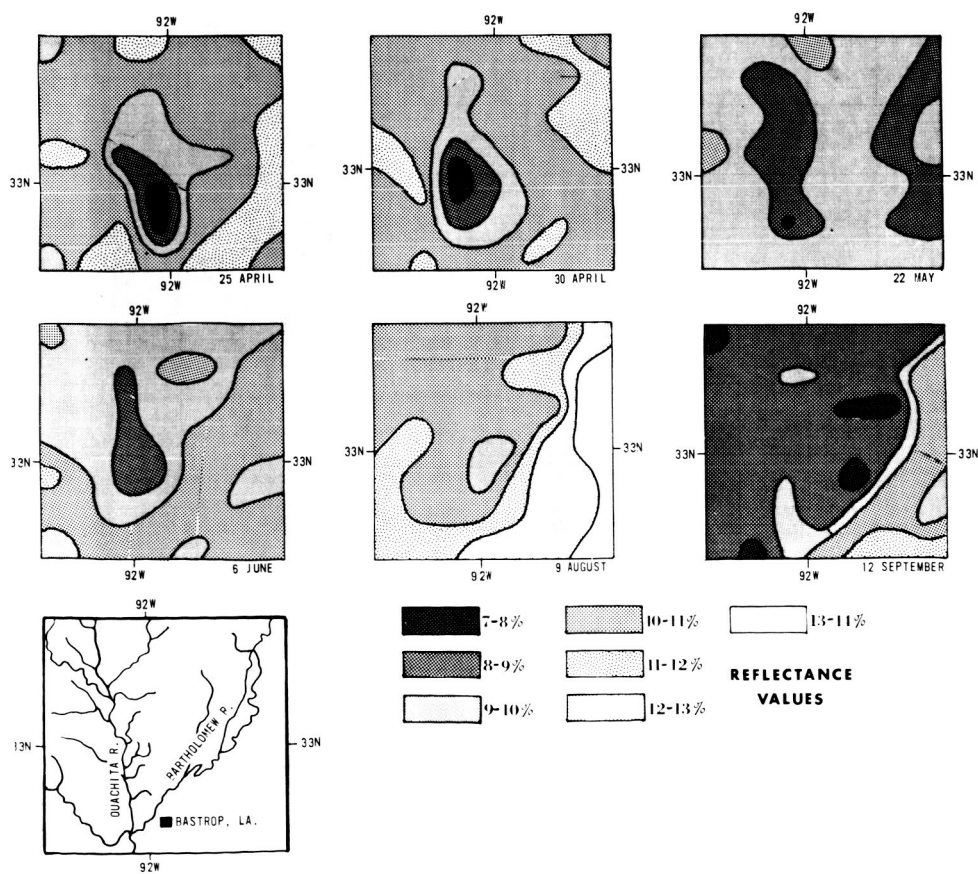


Figure 18. Nimbus III daytime HRIR temporal sequence of reflectance values derived from computer-produced grid print maps. The area is along the Ouachita River at the Louisiana-Arkansas border.

Changes in reflectance values and pattern along the Ouachita correlate with lingering effects of an early spring flood. Some of the other patterns correlate with soil and vegetation patterns.

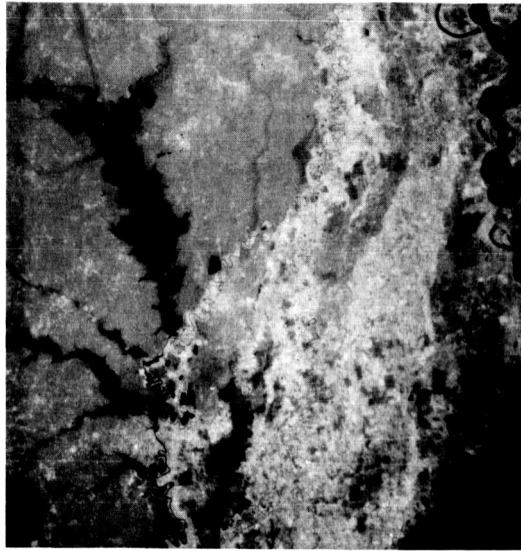


Figure 19. Apollo IX photograph of the lower Mississippi Valley taken on March 9, 1969. The flooded Ouachita River is in the upper left-hand portion of the picture. The highly cultivated flood plains of the Mississippi River occupy the right-hand portion of the photograph (NASA photo).

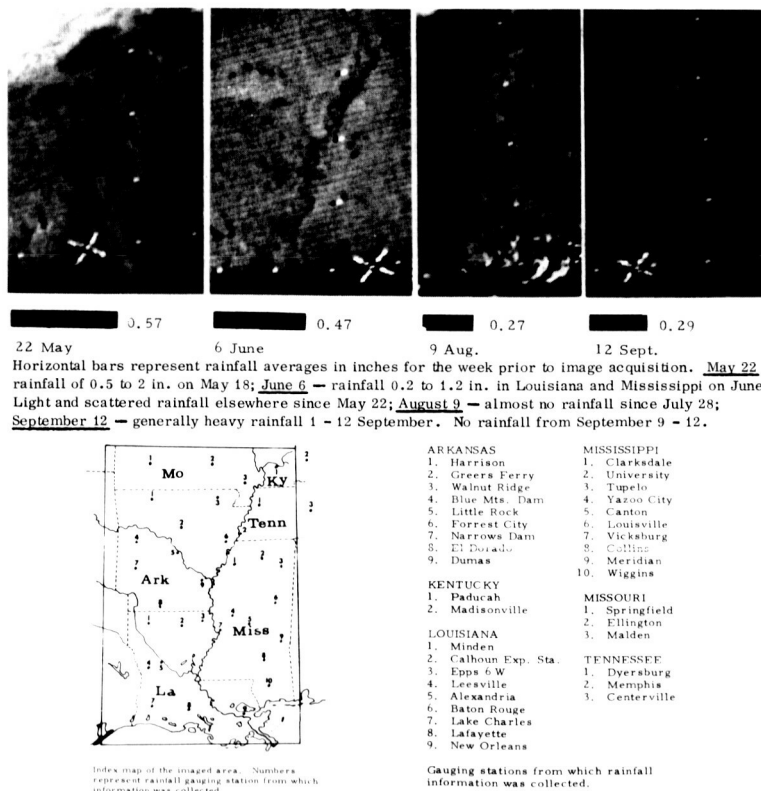


Figure 20. The varying tonal changes in the Mississippi River Valley illustrated here correspond to solar reflectance recorded by the Nimbus III radiometer (daytime HRIR) in the 0.7 to 1.3 μ m band.



Figure 21. Temporal sequence of Nimbus III (day) photofacsimile prints showing western Africa. June 16 - advancing wet season for tropical West Africa; clouds are moving inland from the Gulf of Guinea. July 13 - clouds move inland to approximately 15 deg N latitude; storm gyre over Niger River delta; frontal storms over Jos Plateau and northern Nigeria (above Komadiya-Yube and Sokota River Basins). November 18 - dry season for tropical West Africa. Dust and haze of the harmattan to altitudes of 8000-12 000 ft over the Niger River Basin and northern Nigeria.

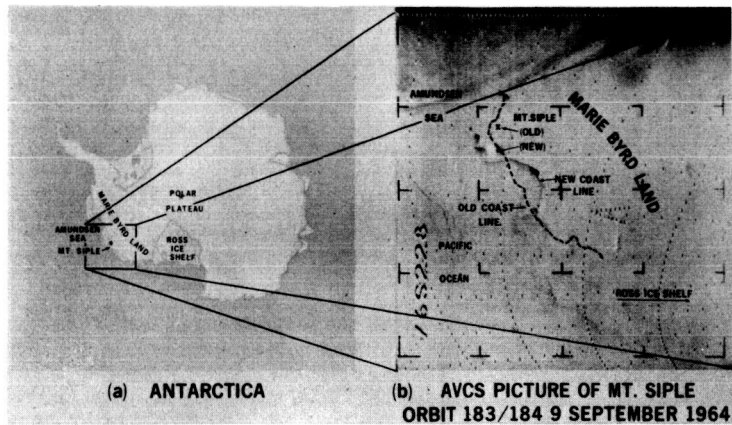


Figure 22. Antarctic map revisions derived from a Nimbus IV picture, recorded on September 9, 1964.



Figure 23. Nimbus I view of the Sayan Mountains and vicinity, U. S. S. R.

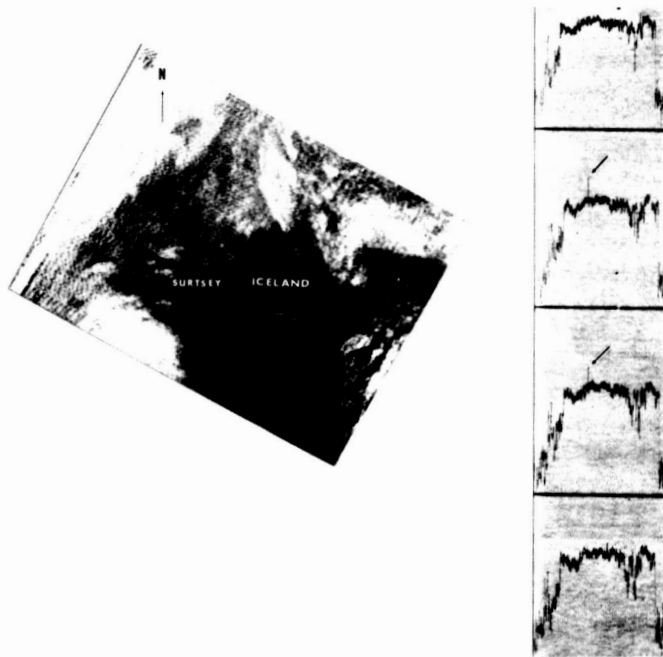


Figure 24. Nimbus II HRIR photofacsimile of Surtsey Volcano observed on September 8, 1966, off the southwestern coast of Iceland. The volcanic eruption shows up as a warm (high) spike on two of the four consecutive analog traces across the Surtsey area.



Figure 25. Ash Plume from Beerenberg Volcano. This new eruption of the Beerenberg Volcano on Jan Mayen Island was first observed on the night of September 20, 1970. By noon on September 21, when this Nimbus IV IDCS picture was taken, the ash plume (within the rectangular area) extended more than 200 mi to the southeast.

F

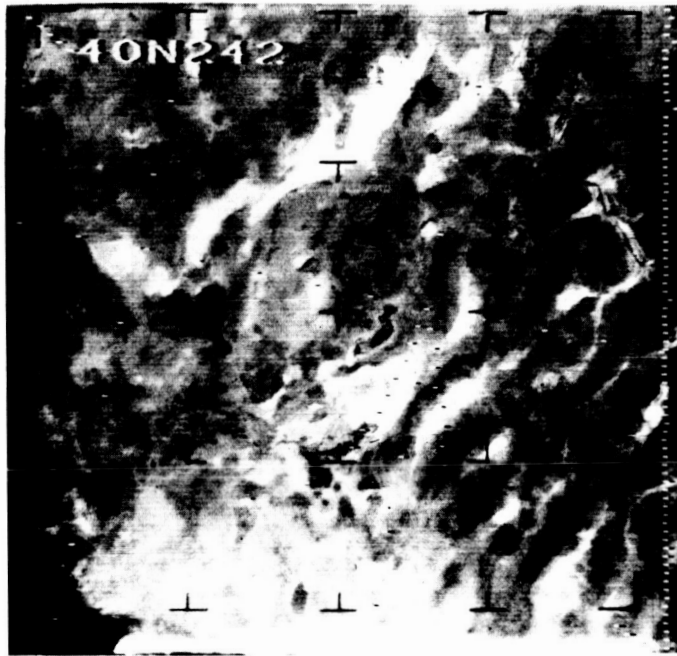


Figure 26. Nimbus I AVCS image, Northwestern Nevada, September 17, 1964. Good contrast separation between lake beds (white and light gray), alluvium (intermediate gray), forested mountains (dark gray), and lakes (black) is apparent.



Figure 27. Gemini V photograph (late August 1965) of Southern Iran. Tashk and Bakhtigam Salt Lakes are clearly delineated (NASA photo).

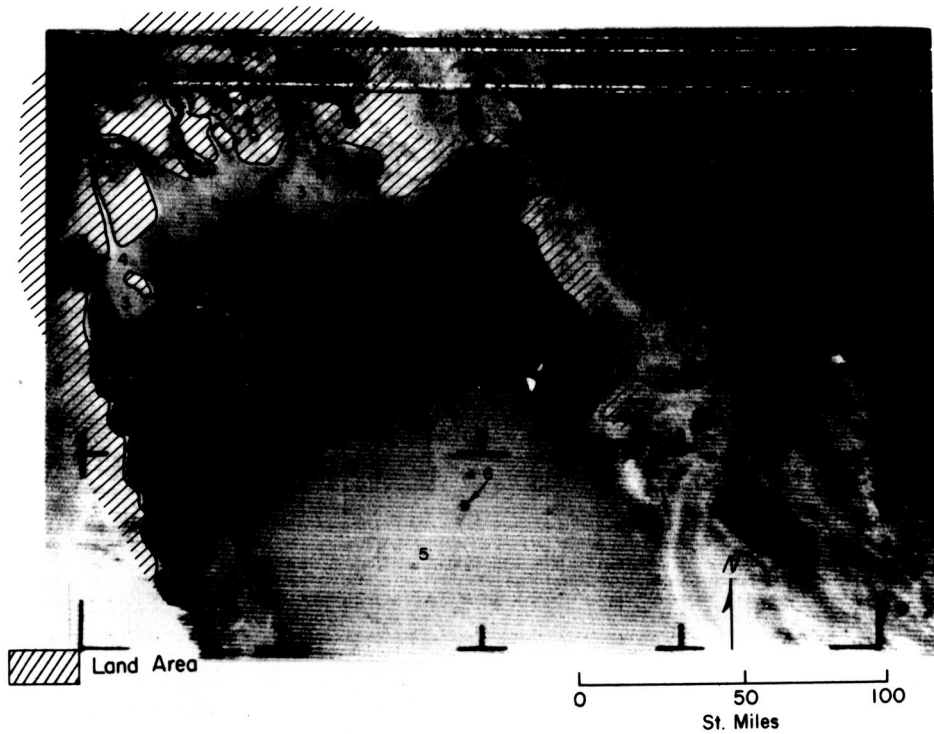


Figure 28. Nimbus I AVCS photograph of the Persian Gulf and the Tigris-Euphrates River Delta. Sedimentation plumes, submerged channels, and other features are identified.

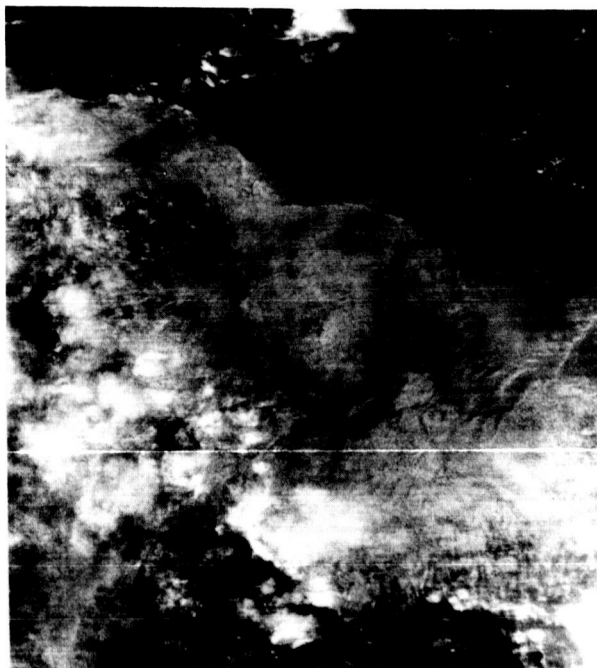


Figure 29. The ATS III view of the Southern Hemisphere. Every 20 min a photograph is taken by the ATS camera, and when the Brazilian coast is cloud free, sedimentation by the Amazon River may be observed on an hourly basis (NASA photo).



Figure 30. An Apollo IX view of the Colorado River's entrance to the Gulf of California. This is a black and white rendition of a color infrared picture of its delta and sediment plumes (NASA photo).

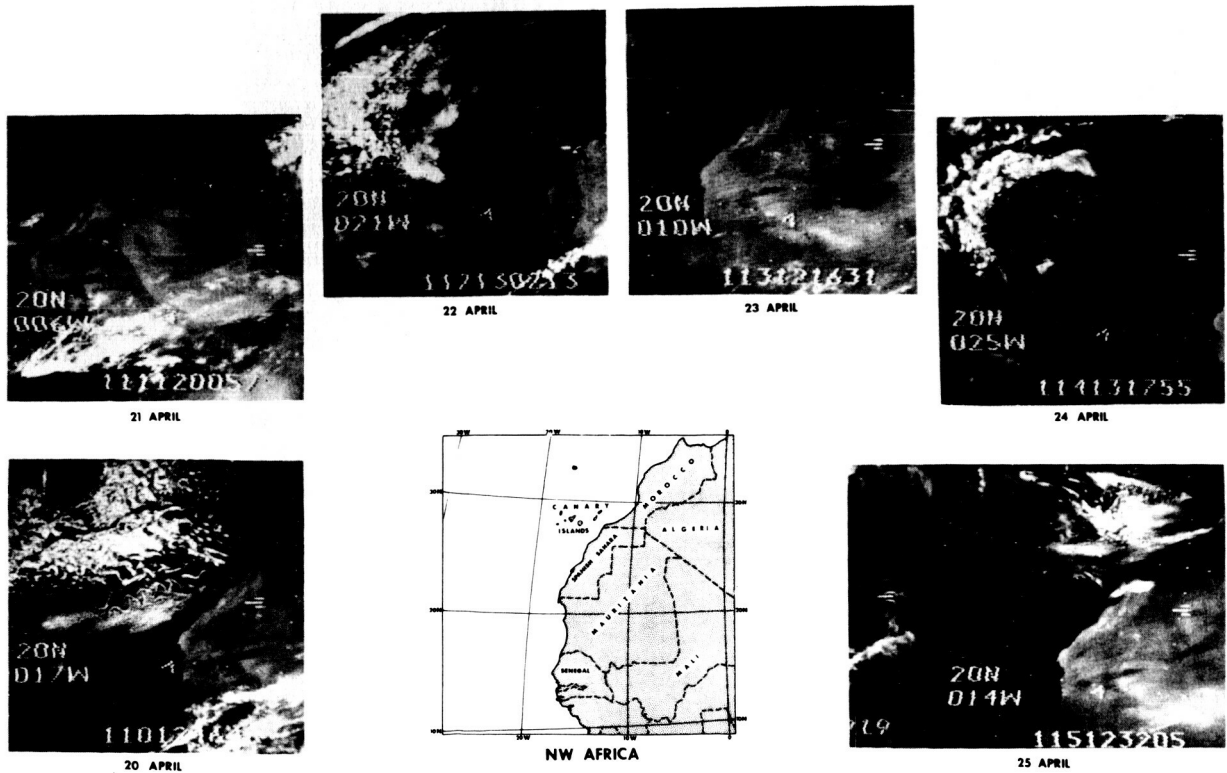
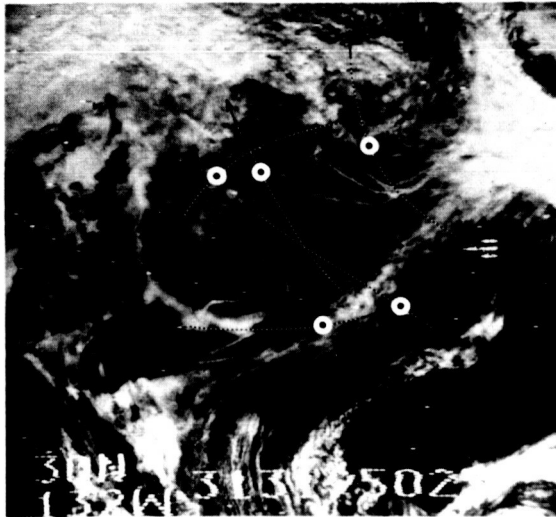


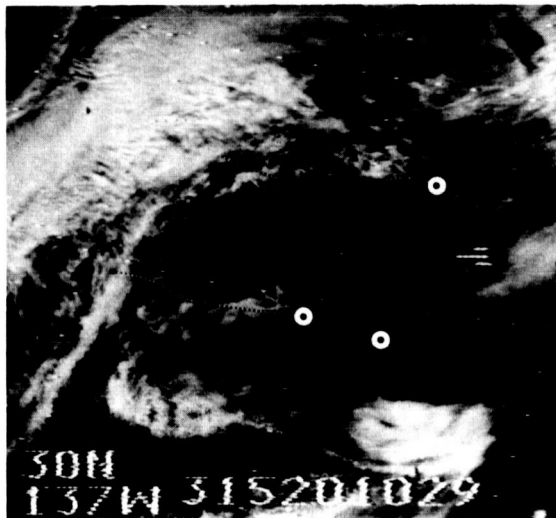
Figure 31. Nimbus IV IDCS monitors 1970 Sahara dust storm.



9 November 1969



10 November 1969



11 November 1969



12 November 1969

Figure 32. Nimbus III IDCS observations of ship plumes. The long, thin, anomalous cloud bands are probably ship plumes.

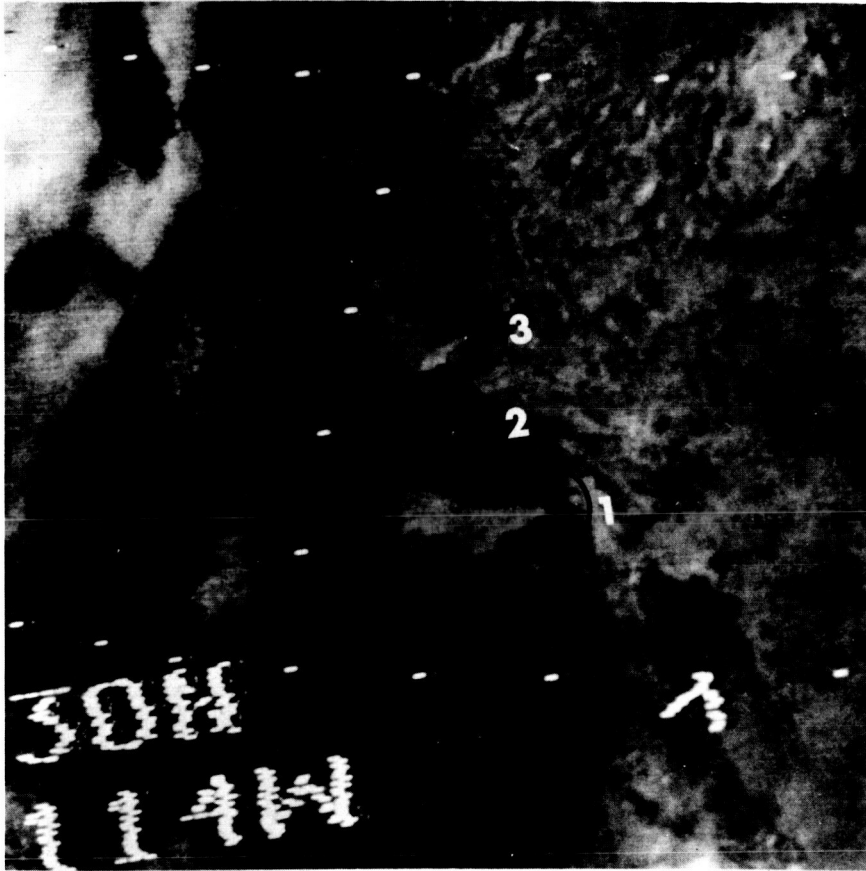


Figure 33. Southern California brush fire smoke plumes. This central portion of a Nimbus IV satellite IDCS picture taken on September 27, 1970, recorded smoke plumes from five of the major brush fires in Southern California. Plume locations are: 1. San Diego - 140 000 acres burning (1 plume); 2. Los Angeles - 105 000 acres burned (3 plumes); 3. Sequoia National Forest - 5000 acres burning (1 plume). (For reference: the Great Salt Lake is in upper right and Salton Sea is just above 1.)

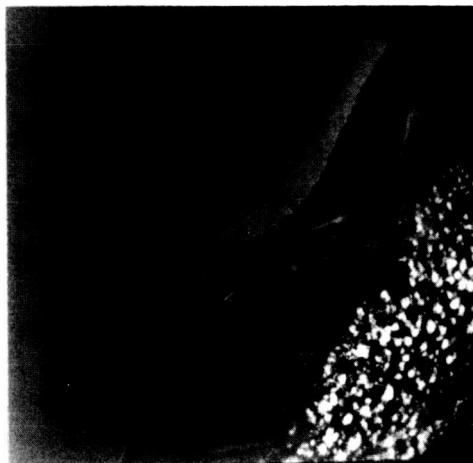


Figure 34. The mouth of the Zambezi River at Mozambique, East Africa. The light arrowlike streaks over the land are smoke and the hues off the shore are produced by sediment (NASA photo).